

TOPICAL REVIEW

Spatially selective photochemical activity on surfaces of ferroelastics with local polarization

To cite this article: Ajay S Pisat *et al* 2017 *Semicond. Sci. Technol.* **32** 103001

View the [article online](#) for updates and enhancements.

Related content

- [Screening mechanisms at polar oxide heterointerfaces](#)
Seungbum Hong, Serge M Nakhmanson and Dillon D Fong
- [Characteristics and controllability of vortices in ferromagnetics, ferroelectrics, and multiferroics](#)
Yue Zheng and W J Chen
- [New modalities of strain-control of ferroelectric thin films](#)
Anoop R Damodaran, Joshua C Agar, Shishir Pandya et al.

Topical Review

Spatially selective photochemical activity on surfaces of ferroelastics with local polarization

Ajay S Pisat , Gregory S Rohrer  and Paul A Salvador 

Department of Materials Science and Engineering, Carnegie Mellon University, PA, United States of America

E-mail: paul7@andrew.cmu.edu

Received 27 March 2017, revised 20 June 2017

Accepted for publication 8 August 2017

Published 4 September 2017



CrossMark

Abstract

Spatially selective surface photochemical reactivity provides charge and half-reaction separation on a surface of a single material, which generally leads to improved photocatalytic performance, including for water-splitting. In this article, we review observations wherein spatially selective reactivity has been observed on the surfaces of two types of ferroic materials: non-centrosymmetric ferroelectrics and, more recently, centrosymmetric ferroelastics. We further propose that there is an interesting connection between these materials. Some ferroelectrics can be described as ferroelastics with aligned dipoles: they are ferroelectric ferroelastics. Centrosymmetric ferroelastics known to exhibit domain selective reactivity can be described as ferroelastics with anti-parallel aligned dipoles: they are anti-ferroelectric ferroelastics. We discuss potential mechanisms for spatially selective reactivity in such anti-ferroelectric ferroelastics. Finally, we identify additional anti-ferroelectric ferroelastics of interest for spatially selective reactivity.

Keywords: photocatalysis, anti-ferroelectrics, ferroelastics, ferroelectrics, BiVO_4 , WO_3 , BaTiO_3

(Some figures may appear in colour only in the online journal)

1. Introduction

Over four decades of rigorous research in the field of solar water splitting and artificial photosynthesis has not yet resulted in an efficient and economical system to produce hydrogen. This fact highlights the intricacy of the problem that stands between us and a carbon-free energy supply. Morrison [1] has formulated a list of six physical attributes to be satisfied by a material to be a potential solar water splitting photocatalyst. Firstly, the band gap of the photocatalysts should be such that they absorb a large part of the solar intensity spectrum, and a lot of research has been carried out on utilizing visible light active photocatalysts [2, 3]. Next, photogenerated charge carriers and half-reaction sites need to be separated. Macroscopic separation is built into photo-electrochemical cells (PECs) [4–6] having distinct electrodes.

Microscopic separation occurs in heterostructured photocatalysts, or materials composed of two or more materials differing in band energies [7–11]. Microscopic separation on the surface of a single material occurs owing to spatially varying internal fields, either from the aligned dipoles of ferroelectrics [12–22] or native surface charges of different surface chemistry [23, 24]. Some photocatalysts are prone to photodegradation, and hence need protection [15, 21, 25–30]. Appropriate energy levels of the conduction and valence bands are a thermodynamic requirement to enable the photocatalyst to oxidize and reduce water simultaneously. Engaging size effects has been shown to be one way of engineering these levels [31]. Lastly, many ingenious nanostructures have been developed by researchers to integrate all of these requirements in a holistic photocatalytic system [32, 33].

A large variety of materials systems have been explored, which fall into the following broad categories—inorganic [34–37], organic [5, 8, 38, 39], inorganic–organic composites [39–41], and bio-inorganic hybrids [42]. Some of these systems have shown tremendous potential for water splitting. 100% photon-to-hydrogen efficiency has been achieved using a CdSe quantum dot embedded asymmetrically in a Pt-tipped CdS quantum rod [37]. A solar efficiency of 5.4% has been reported by combining organic absorbing layers with inorganic co-catalysts [40]. ‘Artificial leaves’ capable of standalone water splitting have been demonstrated using silicon-based semiconductors [36, 43]. Recently, a CO₂ reduction system that exceeds natural photosynthetic efficiencies using *Ralstonia eutropha* bacteria in conjunction with voltage-driven inorganics gave solar-to-chemical fuel efficiencies of 7.1%–9.7% [42].

While these results (and others) show that solar fuel production is extremely promising, none of them are economically competitive in a commercialized technology [44]. Therefore, it is important to continue to develop new materials and new systems for solar water splitting. We have been particularly interested in individual materials that exhibit bi-functional surfaces: surfaces with some regions that preferentially oxidize molecules and other regions that preferentially reduce molecules. Dunn [45] advocated the use of ferroelectric materials for water splitting, and Tiwari and Dunn [22] reviewed photochemistry on ferroelectric surfaces. We later reviewed a broader range of photocatalysts with internal electric fields [12] that promote spatial selectivity of reactions and increase efficiencies by decreasing recombination and back-reaction of intermediates. For ferroelectrics, individual materials that spatially separate reactions, the overlap with the solar spectrum is generally low. The few known solar active ferroelectrics have deficiencies with respect to the other materials criteria. Thus, their utility in solar fuel production is low.

Clearly, a wider range of solar absorbing spatially selective materials is needed. Recently, we found that some centrosymmetric ferroelastics, which are not polar, surprisingly exhibit spatially selective reactivity and absorb visible light. In fact, similar spatially selective surface reactivity was observed on ferroelectrics and centrosymmetric ferroelastics, the first of which is polar in the bulk and latter of which is not. The purpose of this article is to compare the similarities and differences of these distinct materials for photocatalysis, examining mechanisms for domain based reactivity on their surfaces, and discussing paths for their inclusion in solar water splitting systems.

This review (or perspective) is organized as follows. In section 2, we provide a foundation for understanding ferroelastic, ferroelectric, and anti-ferroelectric materials, as well as the basic photodeposition reactions discussed later. In section 3, a summary of domain-based charge separation in ferroelectrics, coated ferroelectrics, and centrosymmetric ferroelastics is given. Section 4 contains a discussion of mechanisms for spatially selective reactivity in each of these materials. Section 5 summarizes the article and provides our

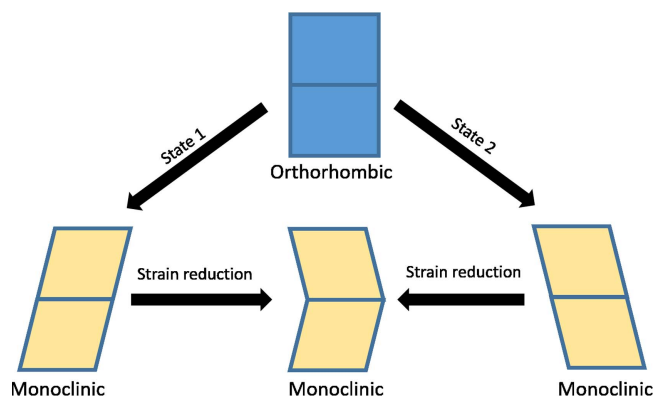


Figure 1. Schematic illustrating domain formation due to a ferroelastic phase transformation (adapted from Wadhawan [142]).

perspective on the potential of anti-ferroelectric ferroelastics in solar water splitting in the light of reports in literature.

2. Foundation

2.1. Ferroics, anti-ferroics, and multi-ferroics

Ferroc materials, such as ferromagnets, ferroelastics, and ferroelectrics, share some common features. They all involve the long-range parallel order of a local vector quantity, namely magnetic moment, strain, and polarization respectively, below a critical temperature referred to as the Curie temperature (T_C). This leads to a net local magnetization, strain, or polarization. Importantly, the ordered vector quantity can be switched between a small number of energetically degenerate directions. Above T_C , either the local order or the magnitude of the vector quantity vanishes, resulting in no order or net value for the vector quantity. Given that this article is based on ferroelastics, let us now consider the ferroelastic transformation.

A schematic of the transformation is given in figure 1, where an orthorhombic high- T structure (all angles are 90°) transforms into a monoclinic low- T structure (the angles are not 90° in this plane). States 1 and 2 are energetically degenerate states, each having the same structure but state 2 is a mirror image of state 1. Generally, the ferroelastic transformation is driven by atomic displacements within the unit cell that lower the overall energy and create a local strain relative to the parent structure.

Multi-ferroics are materials that have more than one type of ferroic order with some coupling between the two order parameters. Many, if not most, ferroelectrics are also ferroelastics. This is because, similar to ferroelastics, a ferroelectric transformation is also driven by ordered atomic displacements. A schematic of local displacements in a ferroelectric is given in figure 2(a); these displacements lead to a polarization because the local center of positive and negative charge is different. In ferroelectrics, these local polarizations order in a parallel fashion. While most ferroelectrics are also ferroelastics, the opposite is not true. This is because ferroelectricity (FE) requires non-

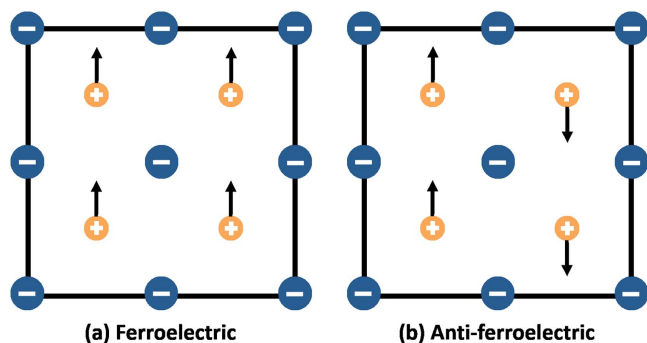


Figure 2. Schematic atomic displacements in (a) a ferroelectric and (b) an anti-ferroelectric. The blue ions with a ‘-’ are negatively charged while the yellow ions with a ‘+’ are positively charged. The black arrows denote the directions of the atomic displacements in both figures.

centrosymmetry, a restrictive crystallographic condition, while ferroelasticity does not. Because both transformations are driven by atomic displacements, they might be expected to be coupled in ferroelectric ferroelastics. The coupling of strain and polarization is obviously interesting for piezotronics.

To minimize the overall energy below T_C , ferroic materials organize into volumetric domains that have the same order direction within a domain, but different order directions across domains. The macroscopic net value of the ordered vector quantity can be zero if the volumes of each type of degenerate domains are equal. A schematic is given in the lower central portion of figure 1, for two unit cells of adjacent domains stacked vertically (state 2 on state 1). Comparing the three lower panels to the parent structure, the central one with two domains is closest to the shape of the parent (and thus has the lowest overall strain energy). In ferroelastics, the crystallographic orientation of the unit cells in a given domain is the same, but changes across domain boundaries.

Domain boundaries in ferroelastics are named with respect to the angular rotation about a low index axis that brings the unit cells in the two adjacent domains into coincidence. The domain boundary (horizontal boundary between the two monoclinic cells constituting the lower central figure) in the schematic of figure 1 is a 180° domain boundary: a 180° rotation about the horizontal axis brings the cells into coincidence. Because the domain boundaries separate regions of distinct crystallographic orientations, the boundary plane is usually subject to significant crystallographic restrictions [46]. Further, most materials are polycrystalline in nature, and a grain typically contains many domains. In much of the photocatalysis work on polycrystalline ferroelectrics, the existence of surface domains allows one to probe the effect of different polarization and orientation states simultaneously.

By the application of an external field, the relative volumes of different domains can be modified, ideally allowing an entire crystal to adopt a single domain (this is called poling). For example, domain switching between energetically degenerate configurations (state 1 and 2 in figure 1) can be carried out by the application of a shear stress. As such, ferroics all exhibit hysteresis in their net

moment versus field plots, which can be understood as the competition between the drive to lower the energy by forming domains and the strength of the local ordering interactions. In photocatalysis, poling [13–15] or local domain writing [47] has been used to correlate the direction of the local polarization to the type of chemical reactivity.

Anti-ferroic materials, such as anti-ferromagnets, anti-ferroelastics, and anti-ferroelectrics, have anti-parallel ordering of their local order vectors below a critical temperature referred to as the Néel temperature (T_N). The anti-parallel alignment results in no net magnetization, strain, or polarization, because the local vector moments cancel out over relatively small length scales. A schematic of atomic displacements in an anti-ferroelectric are shown in figure 2(b). Although there still are local polar units, the net polarization is zero. Interestingly, application of an external field can drive some anti-ferroics into a ferroic state. This is a common expectation for anti-ferroelectrics, whose parallel alignment is only stable under the applied field. One could envision converting the atomic distribution in figure 2(b) to that in figure 2(a), under the correct field. In such cases, the energy difference between the anti-ferroic and ferroic states must be small, as is the case for nearby metastable states. Anti-ferroelectrics do not require non-centrosymmetry, but usually have nearby non-centrosymmetric structures into which they transform in the appropriate field.

Multi-ferroics have two or more ferroic or anti-ferroic order parameters. We are interested here in anti-ferroelectric ferroelastics, which could have interesting coupling between polarization and strain, especially with low-energy ferroelectric structures nearby in phase space. Many good piezoelectrics are solid-solutions with energetically similar ground states of ferroelectricity (FE) and anti-ferroelectricity (AFE) inherited from the parent phases, like PbTiO_3 – PbZrO_3 (FE-AFE). Obviously, the coupling between ferroelasticity, FE, and AFE is well known in the field of piezotronics. Recently, it has come to our notice that this coupling could be important for the design of high performing photocatalysts. We discuss here the use of anti-ferroelectric ferroelastics as a potential class of novel photocatalysts, comparing them to ferroelectric ferroelastics that have been well studied as photocatalysts.

2.2. Correlating reactivity to domain structures

Photodeposition is the process of depositing insoluble metal or oxide nanoparticles on the surfaces of semiconductors submerged in a solution while under illumination by light of a suitable wavelength [48]. Photodeposition can be used for adding functionality to a semiconductor photocatalyst, such as loading it with a co-catalyst for improved reactivity [48] or for examining preferential reaction sites [16, 17, 20, 21, 23, 29, 30, 49–53] by subsequently mapping the location and amount of photodeposited products. This is especially useful in the investigation of heterogeneous surfaces having different grain or domain orientations.

The authors of the reports discussed later have used photodeposition to deposit insoluble silver or lead oxide on

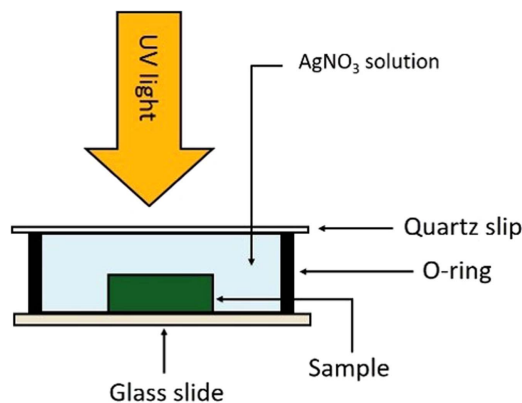


Figure 3. Schematic illustrating the setup for the photodeposition reactions.

photocatalyst surfaces from silver nitrate and/or lead acetate solutions. The Ag^+ ions in the silver nitrate solutions are reduced to elemental silver (Ag) on the surface of the photocatalyst by the photogenerated electrons. Similarly, Pb^{2+} ions in the lead acetate solution are oxidized to Pb^{4+} which are deposited on the surface as PbO_2 particles by the photogenerated holes. These two reactions have been referred to as the ‘Ag photoreduction’ and ‘Pb photo-oxidation’ respectively, throughout the article. In a typical experiment, the photocatalyst is placed within a vessel (e.g., a viton O-ring), which is filled with solution, as shown in figure 3. A quartz slip is used to cover the solution, which allows UV and visible light to pass through. After reaction, the relative quantity and location of photodeposited product can be mapped using optical microscopy, scanning electron microscopy (SEM), or atomic force microscopy (AFM).

To correlate reactivity with the domain structure, the latter needs to be imaged and the polarity of constituent domains needs to be ascertained. The domain structure in ferroelastics can be mapped using SEM (especially using backscatter electron, or BSE, imaging) and AFM. The polarity of domains can be mapped when the domains are piezoresponsive or have different surface work functions by using piezoforce microscopy (PFM) and Kelvin probe force microscopy (KPFM), respectively [54]. In addition to allowing structure and reactivity to be spatially correlated, PFM and KPFM offer the ability to identify specific polarization states of the surface domains.

3. Spatially selective reactivity in ferroelastics

3.1. Ferroelectric ferroelastics

Inoue *et al* [13–15] first studied the effects of ferroelectric polarization on surface properties using coated poled ferroelectric crystals. They showed that O_2 adsorption (surface conductivity) was much higher for NiO films supported on negatively poled (positively poled) LiNbO_3 crystals than for similar films on oppositely poled LiNbO_3 [13]. Additionally, the photocatalytic activity of TiO_2 films supported on poled- LiNbO_3 [15] was enhanced compared to standard

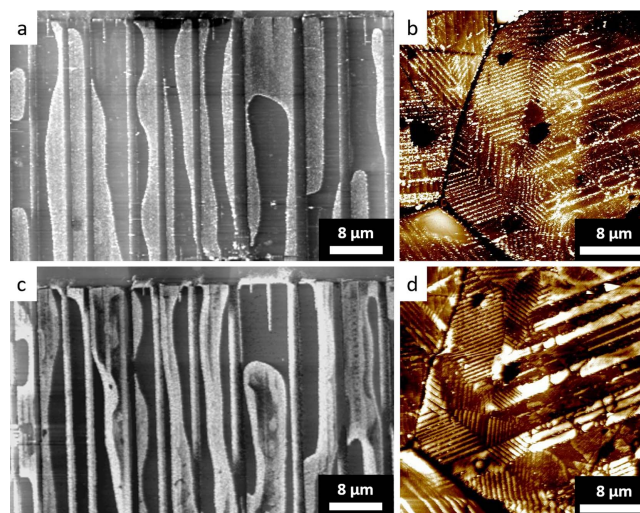


Figure 4. Topography of (a), (c) ferroelectric BaTiO_3 and (b), (d) coated ferroelectric $\text{TiO}_2/\text{BaTiO}_3$ substrates after photodeposition of (a), (b) Ag and (c), (d) PbO_2 . Vertical scales: (a) 100 (b) 55 (c) 110 (d) 80 nm. Figures (a), (c) and (b), (d) are reproduced with permission from [30, 49] respectively.

titania. Later, they also showed that the photocatalytic hydrogen evolution from uncoated lead zirconate titanate (PZT) [14] crystals was 10–40 times higher on positively poled PZT than on negatively poled PZT [14]. All of these observations could be explained by the effects that the ferroelectric polarization had on band bending in the substrate or film, where negative (positive) polarizations lead to upward (downward) band bending in the adjacent substrate or film. Electronic carriers were influenced by these fields, with holes (electrons) attracted to the negative (positive) polarization.

Later, to understand the heterogeneous nature of ferroelectric surface reactivity, we studied the photodeposition of Ag and PbO_2 on unpoled polycrystalline ferroelectrics, including BaTiO_3 [17] and TiO_2 -coated BaTiO_3 [21, 30, 49, 55]. Polycrystalline surfaces having many domains are bi-functional surfaces, with some domains carrying out reduction and some carrying out oxidation. Figures 4(a) and (c) are AFM topography images after Ag photoreduction and Pb photo-oxidation on the same surface of BaTiO_3 . The bright regions in each image are photodeposited solid products. It is immediately clear that the reactivity of the surface is spatially heterogeneous. The reactivity patterns are exactly correlated with the domain patterns of the underlying substrate. Importantly, the regions of the surface that are reactive (unreactive) for reduction in figure 4(a) are unreactive (reactive) for oxidation in figure 4(c). We call this type of bifunctional surface reactivity complementary reactivity: some domains are cathodic and some are anodic. One can describe such a surface as a series of short-circuited PECs dictated by the surface domain structure. Using the polycrystalline nature of the samples, it was shown that similar complementary and spatially selective reactivity was observed across all of orientation space, implying the ferroelectric effects were more important than orientation effects (which are known for other photocatalysts like BiVO_4 [56], SrTiO_3 [57, 58] and NaNbO_3 [59], amongst others).

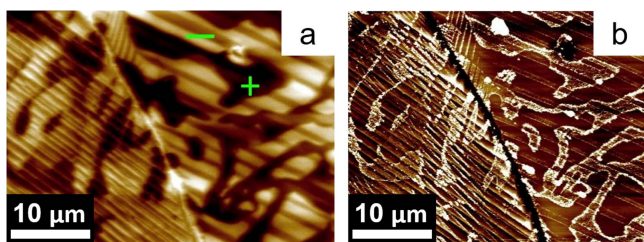


Figure 5. (a) KPFM image of a BaTiO₃ surface. (b) Topography of the same region after Ag photoreduction. Vertical scales: (a) 175 mV and (b) 60 nm. Figures (a), (b) are reproduced with permission from [20].

Unfortunately, many photocatalysts (including BaTiO₃) suffer from photodegradation. A thin stable coating (such as TiO₂) can offer protection from photodecomposition. Figures 4(b) and (d) are AFM topography scans after Ag photoreduction and Pb photo-oxidation respectively on the same surface of TiO₂-coated BaTiO₃. Similar to the bare substrate, the coated ferroelectric exhibits complementary reactivity, with some domains promoting Ag photoreduction and others promoting PbO₂ photo-oxidation. Importantly, for these 15 nm films, the photocathodic (photoanodic) regions of the bare substrate are also photocathodic (photoanodic) regions for the supported film. This is consistent with the mechanism that carriers photogenerated in the ferroelectric substrate are responsible for the reactivity on the non-ferroelectric film surface. The substrate dominated photocatalytic activity of the film was supported by the observations that spatially selective reactivity was independent of the phase of the titania in the film or the orientation of the substrate or film. Of course, the domain influence disappears when the film is too thick [15, 30] and the interfacial charge of the polar domains is screened by the film or the film's absorption is greater than that of the substrate. For example, 100 nm thick films did not exhibit spatially selective patterns of reduced silver [55].

While Inoue *et al* [13–15] were able to pole single crystals to demonstrate the correlation between reactivity and polarization, other methods are needed on the polycrystals. Hu *et al* [60] reported that domains with a positive out-of-plane polarization etched fastest in HCl. These were followed by domains with in-plane polarization. The slowest to etch were the domains which had a negative out-of-plane polarization. Using this method, Giocondi *et al* [16, 17, 49] showed that photocathodic (photoanodic) domains had positive (negative) polarization. They saw that the regions that reduced silver, etched faster in HCl, indicating they had a positive polarization. Higher reactivity implies an enhanced drift of reducing photogenerated electrons towards the surface of that domain, which is consistent with being attracted to positive out-of-plane polarization.

Kalinin *et al* [54] used surface potential microscopy (also known as KPFM) to image the polarity of domains on BaTiO₃. Bhardwaj *et al* [20] followed up by using KPFM to correlate reactivity to domain polarization on BaTiO₃. A KPFM image of the surface of a BaTiO₃ ceramic is shown in figure 5(a), with a grain boundary running slightly off vertical

in the center. In this image, contrast arises from regions having different work functions. Different work functions arise from different near-surface band bending owing to the local dipole moments or charges [19], which in this case correspond to different domain polarizations. The KPFM image maps the ferroelectric domains clearly. An AFM image of the surface after Ag photoreduction is shown in figure 5(b). The photochemical reactivity is clearly correlated with the domains mapped by KPFM. The dark domains in KPFM, which were identified as the positive polarization domains, are photocathodic (reactive for Ag photoreduction), while the light (negative polarization) domains are not. It has been widely reported that ferroelectrics have improved photochemical reactivity in comparison to similar non-ferroelectric materials. Stock and Dunn [61] reported unexpectedly high activity of CO₂ reduction on the surface of ferroelectric LiNbO₃. It was proposed that the strong polarization (70 $\mu\text{C cm}^{-2}$), which shuttles photogenerated electrons and holes away from each other, also leads to very long carrier lifetimes, resulting in the high efficiency. Additionally, the band bending at the surface was considered to allow for charge injection at lower energy levels, adding further to the efficiency. Morris *et al* [62] showed experimentally that the spontaneous polarization in single crystal BaTiO₃ mitigates charge recombination and extends carrier lifetime. Dunn and Tiwari [63] also proposed that ferroelectric polarization leads to a reduction in the photoelectric threshold in LiNbO₃, which is another source of potential improvement. Due to the reduction of the threshold, the photoelectric effect could be engaged to generate free electrons, adding to the increased carrier lifetimes and internal charge separation. In some cases, domain selective adsorption driven reactivity has been reported [64]. In this mechanism, positive (negative) molecules preferentially adsorb to negative (positive) ferroelectric domains. A three-fold increase in photodegradation of rhodamine B was observed for nanophase BaTiO₃ photocatalysts with higher phase ratios of tetragonal to cubic (ferroelectric to non-ferroelectric) BaTiO₃ [65]. The authors have attributed the increased reactivity due to internal charge separation as well as strong polarization-driven adsorption of the dye molecules on the surface.

A fundamental limitation to the use of most ferroelectric photocatalysts for solar energy conversion is that they have wide band gaps and their absorption is limited to the UV region of the solar spectrum. BiFeO₃ is an exception, with a band gap of 2.81 eV [66]. Kalinin *et al* used scanning probe methods to directly write domains of specific polarizations (local poling), and directly demonstrated photocathodic (photoanodic) domains had positive (negative) polarization using PFM [47]. Schultz *et al* [53] carried out photodeposition experiments on ferroelectric BiFeO₃ and correlated reactivity with polarization using PFM. The PFM out-of-plane phase difference is shown in figure 6(a), which shows clear polygonal piezoresponsive domains. The topography of the same area after Ag photoreduction with blue light is shown in figure 6(c). The bright regions in figure (c) are coated with Ag, and these correspond to the dark domains in the PFM image of figure 6(a). Even for the solar absorbing

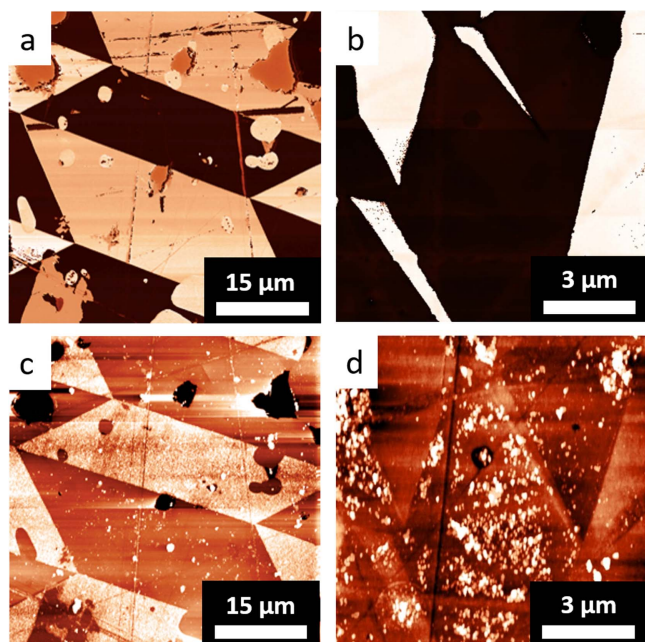


Figure 6. (a) and (b) PFM images (out-of-plane phase difference) of (a) ferroelectric BiFeO₃ and (b) TiO₂ coated ferroelectric BiFeO₃. (c) and (d) AFM topographic images after Ag photoreduction. Dark to bright vertical scales are: (a) 180° to 0°, (b) 180° to -180°; (c) 0–60 nm and (d) 0–15 nm. Figures (a), (c) and (b), (d) are reproduced with permission from [29, 53] respectively.

BiFeO₃, it was shown that reactivity on certain domains was greater than others and that the influence of domain polarization overwhelmed effects of crystallographic orientation.

Zhang *et al* [29] carried out similar photodeposition investigations on TiO₂-coated BiFeO₃. As was the case for other coated ferroelectrics, when the film was thin (10 nm), spatially selective reactivity was observed. The PFM out-of-plane phase difference of the coated BiFeO₃ system is shown in figure 6(b). The topography of the same area after Ag photoreduction with blue light is shown in figure 6(d). The bright regions in figure (d) are coated with Ag, and these correspond to the dark domains in the PFM image figure 6(b). Because TiO₂ does not absorb visible light, the primary photo-generation of charge carriers takes place in the ferroelectric substrate. The substrate domain polarization then influences the drift of photogenerated carriers to the film/substrate interface. The carriers then traverse the coating and react at the TiO₂ surface in patterns identical to those of the substrate. Notably, a small maximum polarization of 6.1 μC cm⁻² exists along the <111> direction of BiFeO₃ [53]. Hence, for any other orientation, the out-of-plane component is expected to be even smaller. This smaller component was seen to be enough to influence reactivity through a 10 nm film of TiO₂ [29]. Hence, it suggests that smaller polarizations below 10 μC cm⁻² are enough to drive spatially selective reactivity on photocatalysts coated with thin films.

3.2. Anti-ferroelectric ferroelastics

The prior section discussed spatially selective reactivity in ferroelectrics, driven by spatial differences in surface band

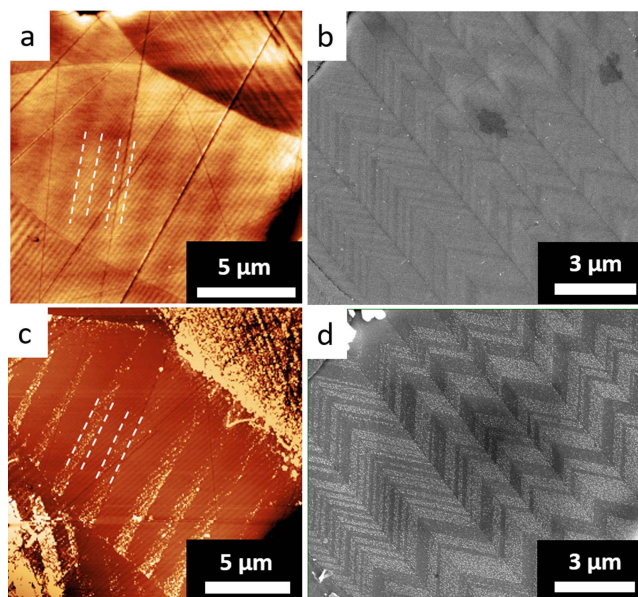


Figure 7. (a) AFM topographic image of BiVO₄ and (b) secondary electron (SE) image of WO₃ surfaces, both before reaction. (c) AFM topographic image of BiVO₄ and (d) SE image of WO₃, both after reaction and from the same areas as (a) and (b). Figures (a), (c) reproduced with permission from [52].

banding related to domain polarization. Notwithstanding BiFeO₃, ferroelectrics are mostly UV absorbing materials. Recently, it was shown that some non-polar solar absorbing ferroelastics also exhibit spatially selective photochemical activity that is analogous to ferroelectric photochemical surface reactivity. Munprom *et al* [52] were the first to report spatially selective reactivity on BiVO₄, a centrosymmetric ferroelastic. BiVO₄ exhibits ferroelasticity on cooling through a phase transformation from the tetragonal scheelite to the monoclinic fergusonite structure at 255 °C [67]. Ferroelastic BiVO₄ is centrosymmetric and potentially anti-ferroelectric [68]. The ferroelastic domains are clearly observable by AFM, as shown in figure 7(a). When Ag photoreduction was carried out using UV light or blue LEDs, the surface reactivity was observed to be correlated to the ferroelastic domain structure, as shown in figure 7(c) [52]. The domain structure of BiVO₄ is complex, and only some of the domains promote Ag photoreduction, which is apparent in the central grain of figures 7(a) and (c). The set of domains highlighted with white lines are photo-active. Within those photo-active domains, the other set of domains modulates the reactivity, reinforcing the importance of the ferroelastic domains on surface reactivity.

Very recently, we reported similar spatially selective reactivity for centrosymmetric ferroelastic WO₃ [69]. WO₃ undergoes two ferroelastic transformations: a tetragonal to orthorhombic (α -WO₃ \rightarrow β -WO₃) one at 740 °C and an orthorhombic to monoclinic (β -WO₃ to γ -WO₃) one at 310 °C [70, 71]. Similar to BiVO₄, γ -WO₃ is a centrosymmetric anti-ferroelectric ferroelastic [72–74]. The dual transformation leads to a complex hierarchical domain structure, two levels of which are apparent as chevron patterns shown in figure 7(b). After carrying out Ag photoreduction, a clear

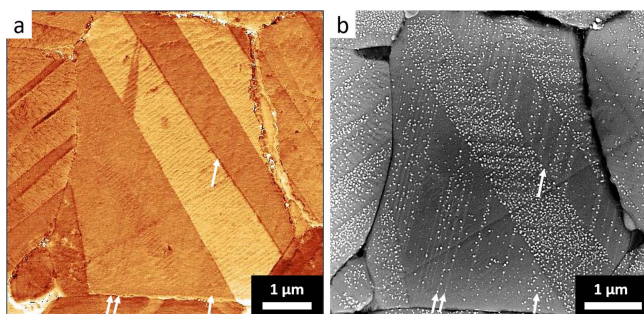


Figure 8. (a) PFM image of γ - WO_3 and (b) SEM image after Ag photoreduction. The white arrows mark the same secondary domains in both figures. Vertical scale: (a) 37° . Figure reproduced with permission from [69].

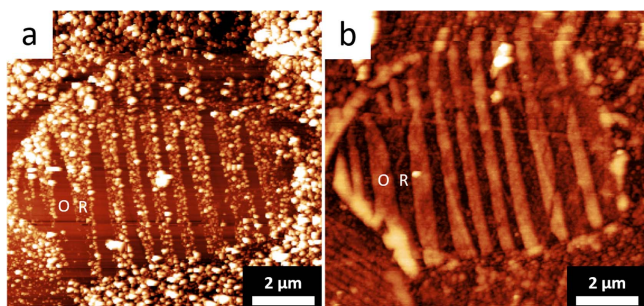


Figure 9. Topographic AFM images of BiVO_4 after photodeposition of (a) Ag and (b) MnO_2 . 'O' indicates the oxidative domains whereas 'R' indicates the reductive domains. Vertical scale: (a) 80 nm (b) 150 nm. Figure reproduced with permission from [51].

correlation of the spatially selective surface reactivity to the underlying domain structures was found, as shown in figure 7(d).

While this spatially selective photochemical reactivity is similar to that on ferroelectrics, centrosymmetric ferroelastic domains are not expected to have polar surfaces. To determine whether the surfaces of BiVO_4 and WO_3 were polar, they were imaged by PFM. As illustrated in figure 8(a), γ - WO_3 exhibits surface piezoresponsivity. This implies that the surfaces of γ - WO_3 are polar, even though the bulk is not. A polar surface response was first reported for heavily reduced WO_3 [75] and later for epitaxial γ - WO_3 (100) surfaces [74]. The reaction pattern after Ag photoreduction is shown for the same area in figure 8(b), and there is a clear correlation between the PFM domains and the reactive domains, suggesting that the piezoresponse (or polarity) drives the spatially selective reactivity.

The micrographs in figure 9 illustrate the complementary characteristic of the photochemical reactivity on the surface of BiVO_4 . Figure 9(a) shows the domain selective reactivity for Ag photoreduction, while figure 9(b) shows MnO_2 photo-oxidation on the same area. This surface had clear piezoresponsivity and complementary photochemical reactivity that correlated directly with the surface polarity. In contrast to the ferroelectric ferroelastics, wherein the polarization was the dominant driving force, both crystal orientation and domain type were important for spatially selective reactivity on BiVO_4 [51]. Spatially selective reactivity was observed over

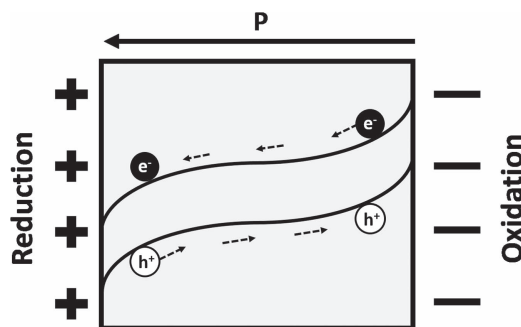


Figure 10. A schematic of the 1D polarization driven photochemical reactivity for a ferroelectric.

the entire orientation space. However, surfaces closer to (001) plane were more active for Ag photoreduction.

Finally, Munprom *et al* [51] showed that the spatially selective photochemical reactivity improved the net reactivity for co-doped BiVO_4 . Using photodeposition experiments, they compared the reactivity of Na- and V- co-doped samples of BiVO_4 on either side of the composition dependent phase boundary. It was shown that higher reactivity was observed on the monoclinic sample, which had piezoresponsive surfaces, than on the tetragonal sample, which did not have piezoresponsive surfaces. Overall these observations indicate that surfaces of monoclinic BiVO_4 and γ - WO_3 are polar, and the local polarization is large enough to influence surface photochemical activity, resulting in complementary reactivity similar to that observed in ferroelectrics.

4. Potential mechanisms and evidence

4.1. Computational models of ferroelectric photocatalysis

Spatially selective reactivity has been widely observed on ferroelectrics, as described above, and ferroelectrics are known to improve the net efficiency for many photochemical reactions [62, 65, 76]. The primary models used to account for these observations are that screening the ferroelectric polarization internally causes surface band bending or externally causes preferential adsorption. Sub-surface band bending results in internal fields that separate charge carriers and enhance carrier lifetimes. A one-dimensional (1D) schematic of this polarization driven surface reactivity is shown in figure 10. The positive (negative) polarization at the surface bends bands downward (upward) in the near surface bulk, representing an internal electric field. In the schematic, the length is equal to the sum of the two space charge regions on either side of the particle (hence the bands are not flat anywhere in the schematic). Carriers photogenerated in the space charge regions are driven in opposite directions: holes (electrons) to the negatively (positively) polarized surface. Whether a carrier driven away from the surface traverses the bulk and arrives at the opposite surface depends on the size and electronic transport properties of the material. The question arises: what is the maximum quantitative effect that

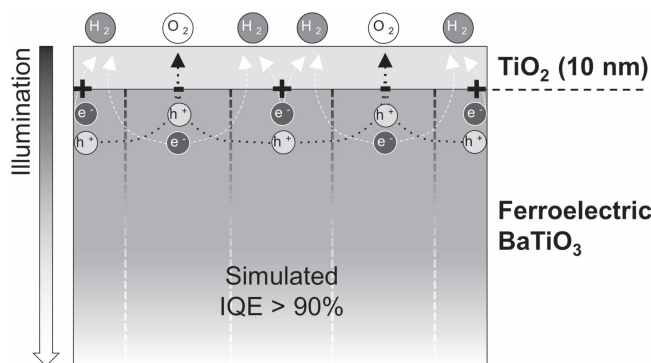


Figure 11. A schematic of the 2D polarization driven photochemical reactivity for a ferroelectric with a thin anatase coating. Figure reproduced with permission from [78].

this mechanism can have on the overall photocatalytic efficiency?

Recently, the internal quantum efficiency (IQE) was modeled computationally for a 1D coated ferroelectric [77]. The structure was a single-domain poled electrode with only one surface modeled as a reactive surface. The model was also used to explore the effects on the IQE caused by a number of independent parameters, including majority carrier kinetics, film thickness, applied potential, minority carrier lifetime, and ferroelectric polarization. The most important observation was that an IQE >90% was attainable for specific combinations of parameters whose values were all physically reasonable.

One important question is, of course, how does the value of surface polarization impact properties? Polarization values for ferroelectrics can vary from a few to a hundred $\mu\text{C cm}^{-2}$. The polarization for BaTiO_3 (P_{BTO}) is $\approx 26 \mu\text{C cm}^{-2}$. Glickstein *et al* [77] used the 1D computational model to vary the surface polarization from zero to $2P_{\text{BTO}}$. They observed that the most significant improvement occurred for the initial increase in polarization from a neutral surface ($0 \mu\text{C cm}^{-2}$) to that having $\frac{1}{4}P_{\text{BTO}}$ ($\approx 7 \mu\text{C cm}^{-2}$). The initial jump in polarization (from 0 to $\frac{1}{4}P_{\text{BTO}}$) corresponded to an increase in IQE by a factor on the order of 5–100. Further increasing the polarization value from $\frac{1}{4}$ to $2P_{\text{BTO}}$ increased the IQE by only a factor on the order of 2–5. This indicates that the largest improvement may be the initial increase in polarization, indicating that even low polarization values on the order of $5\text{--}10 \mu\text{C cm}^{-2}$ may be interesting for highly efficient photocatalysts. Depending on the origin of surface polarization in anti-ferroelectric ferroelastics, their surface polarizations may be in this range.

Glickstein *et al* [78] followed up that study with a 2D model that simulated the surface of a coated ferroelectric having 180° domains of finite and equal widths. The model was designed to assess the physical experiments discussed relative to figure 4(b), for TiO_2 -coated BaTiO_3 . When modeling the experimental conditions of anatase TiO_2 on BaTiO_3 , the IQE was computed to be less than 1%. Again, by optimizing the relevant parameters, an IQE of over 90% could be obtained on the single surface having oxidation and reduction occurring on spatially separated domains.

A schematic of this is shown in figure 11. Holes photo-generated in the positive domains are shuttled towards the

negative domains flanking them. Conversely, electrons photo-generated in the negative domains are shuttled towards the positive domains flanking them. In the photolysis of water, domains shuttling electrons (holes) towards the surface promote the hydrogen evolution reaction (oxygen evolution reaction), as marked in figure 11. In order to obtain the highest IQEs, domains must be sufficiently wide to allow for full space charge layers to develop (a few tens of nm) but sufficiently narrow to allow for carriers shuttled away from the surface in one domain to successfully migrate to the surface in an adjacent domain for reaction (a few hundreds of nm). For domains with widths in the range of $\approx 50\text{--}400$ nm (in BaTiO_3), the IQE was on the order of 90% of the maximum IQE for a specific set of conditions, indicating a reasonable range of domain sizes can provide near-optimal performance.

In contrast to ferroelectrics, ferroelastic BiVO_4 and WO_3 , which also show spatially selective reactivity, are centrosymmetric and non-polar. In other words, there is no bulk polarization that can impact surface properties as in the models described here. Therefore, there is no immediately obvious mechanism to explain why ferroelastic surface domains are polar and piezo-responsive, and how the domains lead to spatially selective and complementary reactivity. However, two mechanisms have been proposed to explain the origin of polarization:

- Flexoelectricity from surface strain gradients
- FE from a surface phase transformation

4.2. Surface flexoelectricity

Flexoelectricity is a physical phenomenon wherein a strain gradient in a crystal causes a dipole moment [79]. Unlike FE, flexoelectricity is not restricted by the crystallography of the material [79]. A flexoelectric polarization is possible even in centrosymmetric materials. Because strain gradients are likely to exist at surfaces, there have been many studies of surface flexoelectricity.

Munprom *et al* [52] proposed that two kinds of stress relaxations could contribute to flexoelectric polarization at the surface of ferroelastic domains. The first arises from surface restructuring owing to the high energy of the bulk terminated structure, and the degree of freedom associated with the free surface (in principle, surface piezoelectricity could arise in a similar fashion). This can result in a surface strain gradient normal to the surface on the unit cell level, a common description of the origin of flexoelectricity in materials. A schematic is shown in figure 12 [52]. In the schematic, the relative displacements of the Bi ions are shown, along the c -axis of the fergusonite structure. Atoms closer to the free surface are displaced further than atoms far from the surface, which more or less retain their bulk positions. This difference in the magnitude of shift of position of atoms will give rise to a strain gradient, which will in turn contribute to polarization via flexoelectricity. In figure 12(a) (figure 12(b)), the bismuth ions displace away from (towards) the free surface resulting in

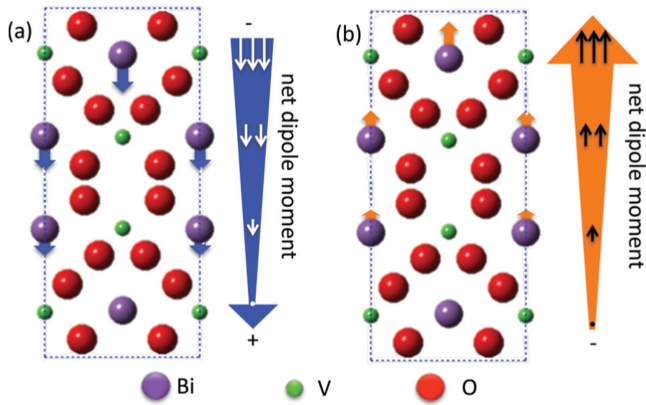


Figure 12. Differential displacement of bismuth ions (a) away from the surface—downward dipole moment (b) towards the surface—upward dipole moment. Figure reproduced with permission from [52].

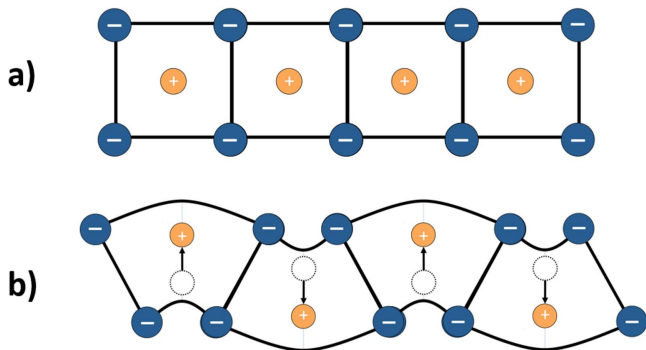


Figure 13. (a) Unstrained free surface before domain formation, (b) development of undulations and alternately polarized domains after strain relaxation at free surface. Figure is adapted from [79, 143].

negative (positive) flexoelectric polarization from the surface strain gradients.

The second relaxation proposed to explain surface flexoelectricity is associated with residual transformation strains from the ferroelastic phase transformation. Domains form during the ferroelastic transformation from tetragonal to monoclinic BiVO_4 to minimize the overall volumetric strain (see figure 1) energy. For a polycrystalline surface, in which each grain (or crystal) is mechanically attached to the surrounding grains of different orientations, not all of the transformation strain can be fully relaxed. The residual transformation strain can be somewhat accommodated at the free surface. A schematic of a free surface is shown in figure 13. A free surface before surface relaxation is shown in figure 13(a), while surface undulations due to surface relaxation are shown in figure 13(b), and how these could lead to alternating dipole moments. The undulation is exaggerated in the schematic to alternate every unit cell, to describe the atomic displacements. However, the specific surface relaxation is related to the local stress states in such a model, which are ultimately determined by the domain and grain structure. If the relaxation couples to the domain

structure, which exists to alleviate strain energy, then one could envision spatially selective reactivity, with the polarity changing on the period of domains [79]. It should be noted that surface relaxations are also a function of the orientation of the grain and, hence, they may not always result in appropriate strain gradients or alternating polarizations. The net dipole from flexoelectricity in many materials is generally rather small, being a function of the material's coupling constant between polarization and the magnitude of the strain gradient. Materials with large coupling constants often have internal dipolar units or are susceptible to the formation of polar units, such as ferroelectrics and related dielectrics, including incipient ferroelectrics, anti-ferroelectrics, and relaxor ferroelectrics. Typical polarization values are on the order of a few $\mu\text{C cm}^{-2}$ for materials with large coupling in reasonable strain gradients. The observation that the tetragonal phase of co-doped BiVO_4 does not exhibit intragranular spatial selectivity or piezoresponsiveness at the surface indicates that the ferroelastic transformation to the monoclinic structure is key for surface polarization [51]. The monoclinic BiVO_4 structure can be described as anti-ferroelectric, as can the $\gamma\text{-WO}_3$ structure. In both, local polar groups are oriented in an anti-parallel fashion. At the surface, where long-range periodicity is broken, the anti-polar displacements are also locally perturbed. It is of interest then, to understand the potential coupling between the anti-polar structure, surface relaxation, residual transformation strains, and ferroelastic domain structure, to understand if significant enough flexoelectric coupling can explain the surface photochemical properties. The computations from Glickstein *et al* [77, 78] indicate that a reasonable value of flexoelectric polarization, in the range of a few $\mu\text{C cm}^{-2}$, is enough surface polarization to modify reactivity significantly.

4.3. Surface FE

One of the interesting features of an anti-ferroelectric is that an applied electric field can induce a phase transition into a ferroelectric state [80], in which the anti-parallel alignment becomes a parallel alignment of local dipoles. Anti-ferroelectric to ferroelectric phase transitions are well documented in thin films, induced by epitaxial strain [81–84] and surface terms [84]. All of these occur because of the relatively small energy differences between the polar and non-polar structures (parallel and anti-parallel dipole alignments) [80, 85, 86]. Thus, a second potential origin of the polar surface states and spatially selective reactivity observed for WO_3 (and possibly BiVO_4) is that the surfaces undergo a phase transformation to a ferroelectric polar state, from their bulk anti-ferroelectric structures.

Interestingly, a ferroelectric phase transition has been induced in anti-ferroelectric $(\text{Pb}_{0.97}\text{La}_{0.02})(\text{Zr}_{0.90}\text{Sn}_{0.05}\text{Ti}_{0.05})\text{O}_3$ films as a result of an adjacent Ni–Mn–Ga shape memory alloy undergoing a ferroelastic phase transition [87]. This indicates that a ferroelastic strain can be large enough to drive a thin adjacent anti-ferroelectric layer to a polar state. One can thus envision that the polished surface of an anti-ferroelectric

ferroelastic is susceptible to a surface phase transition on cooling through its own ferroelastic phase transition, owing to the degrees of freedom at the surface. Recently, the origin of AFE in PbZrO_3 has been described as being stabilized from flexoelectric coupling [88]. Thus, a surface strain gradient provides another potential factor that influences the competition between polar and anti-polar phases.

WO_3 shows an anti-polar dipole arrangement [72] and has been recognized as an anti-ferroelectric [80, 89]. Additionally, $\epsilon\text{-WO}_3$ is a stable ferroelectric phase below -40°C , or $\approx 70^\circ\text{C}$ below room temperature [90]. The presence of an energetically similar ferroelectric phase could allow for a polar surface phase to develop, that would explain its ferroelastic spatially selective reactivity. Alternating surface stress states could stabilize different orientations of the dipoles in the polar surface phase. BiVO_4 is not generally described as an anti-ferroelectric, but structurally it meets the crystallographic requirements to be categorized as one [68]. Because a polar phase has not been previously reported nor computationally investigated (yet its existence is allowed by crystallography [68]), the observation of a polar surface phase would be more surprising in BiVO_4 than in WO_3 .

5. Summary and outlook

In section 3.1, we reviewed the observations that uncoated and coated ferroelectric materials exhibit spatially selective surface photochemical reactivity. Polarization driven charge separation leads to spatially selective reactivity that enables both photocathodic and photoanodic reactions to take place on different regions of a surface of a single material. In section 4.1, we reviewed recent computational work demonstrating that IQEs of 90% are possible by adjusting the domain widths, polarization, and reaction conditions (e.g. pH) of such materials. Thus, having both electrochemical reactions occur on distinct, organized regions on a single surface can be highly beneficial for achieving solar water splitting. However, the number of ferroelectric materials is limited: they must belong to one of only 10 of 32 crystallographic point groups [134]. Further, the number of ferroelectric materials that absorb visible light limits the number of ferroelectric solar water splitting photocatalysts [53, 135, 136].

In section 3.2, we reviewed recent observations for spatial separation of photochemical reactions on solar absorbing ferroelastics. Ferroelastic BiVO_4 and WO_3 both exhibit domain selective reactivity and polar surface properties, as if the surfaces were ferroelectric. In sections 4.2 and 4.3, we discussed two likely sources of surface polarity in BiVO_4 and WO_3 : surface flexoelectricity and surface FE. In either case, one might expect the surface polarization to be lower than that of a strong ferroelectric, but the computation discussed in section 4.1 indicates values on the order of $5\text{--}10\ \mu\text{C cm}^{-2}$ should be sufficient to improve the IQE, in qualitative agreement with the beneficial effect of spatial selection reported for co-doped BiVO_4 .

In principle, flexoelectricity can arise in any crystalline material (i.e., there are no crystallographic restrictions). Further, because the surface causes a break in inversion symmetry (the surface is not centrosymmetric by definition), polar surface states (surface piezo-electricity or FE) can exist even in centrosymmetric materials. This potentially opens the door to search for similar effects in a host of materials. Ferroelastics are of particular interest because they are abundant in nature (more than 30% of the earth's crust is made up of ferroelastic materials [137]) and they exhibit well-defined domain structures conducive for spatially selective reactivity.

It should be clear from our discussion that the nature of these surface charges on centrosymmetric ferroelastics remains an open question. However, the magnitude of the polarization at their surface is expected to be coupled to the material's ability to polarize under a given strain state. Throughout the article, we emphasized the fact that both WO_3 and BiVO_4 have local dipolar units within a unit cell that have anti-parallel alignment: they can be considered anti-ferroelectrics. We propose that the observed surface polarity and spatially selective reactivity originate from the coupling of ferroelastic transformation strains with surface relaxations associated with the local ordering (surface flexoelectricity) or long range ordering (surface FE) of dipoles near the surface.

We think anti-ferroelectric ferroelastics represent an interesting new class of materials that can have spatially selective reactivity, exhibit improved IQEs relative to the neutral surfaces, and may offer a wider range of solar absorbing materials for which band alignments may prove favorable. Table 1 lists some potential anti-ferroelectric ferroelastics whose surface photochemical properties are worth investigating. In other words, spatially selective reactivity could also be expected on the surfaces of these materials. In addition to those compounds which have already been studied, BiNbO_4 , BiTaO_4 and AgNbO_3 seem promising candidates for solar water splitting considering their relatively small band gaps. These materials have all been studied previously as solar active photocatalysts: BiNbO_4 [138, 139], BiTaO_4 [140], and AgNbO_3 [141]. However, other than the reports on BiVO_4 and WO_3 discussed above, there have been no reports on the spatially selective reactivity of these ferroelastics.

6. Conclusions

Spatially selective reactivity has been widely reported for room temperature ferroelectrics, such as UV-active BaTiO_3 and solar-active BiFeO_3 , as well as for these (and other) ferroelectrics coated with non-ferroelectrics. By optimizing materials parameters, domain structures, and reaction conditions, IQEs much greater ($\approx 90\%$) than Z-scheme methods (maximum of 50%) are attainable for a given ferroelectric surface. Recently, non-polar ferroelastic BiVO_4 and WO_3 were reported to have ferroelastic spatially selective reactivity correlated with surface polarity. While the origin of the surface polarity is an open question, as is

Table 1. List of anti-ferroelectric ferroelastic photocatalysts which could show domain specific photoactivity.




Compound	Ferroelasticity	Band-gap (eV)	Anti-ferroelectricity	Comments
BiVO ₄	[67]	2.4–2.5 [91]	[68]	Scheelite family. Fulfills symmetry conditions for anti-ferroelectricity. Characteristic double P–E loop experiments not carried out
WO ₃	[71, 73, 74]	2.4 [92] 2.4–2.8 [93]	[72, 80]	Distorted—perovskite structure. Fulfills symmetry conditions for anti-ferroelectricity. Characteristic double P–E loop experiments not carried out
BiFeO ₃	[94]	2.81 [66]	[80, 95, 96]	Perovskite family. Ferroelectric phase stable at Room temperature
BaTiO ₃	[97]	3.2 [20]	[98–100]	Ferroelectric phase stable at Room temperature
BiNbO ₄	[101]	2.6 [102]	[103]	Stibiotantalite structure
BiTaO ₄	[101]	2.45–2.8* [104]	[105]	*-computational band gap
LaTaO ₄	[106]	2.7 [102] 3.8 [107]	[108]	A _n B _n X _{3n+2} layered perovskite family
BaMnF ₄	[109]	3* [110]	[111, 112]	A _n B _n X _{3n+2} layered perovskite family
NaNbO ₃	[113–115]	3.27*(undoped) 2.46–2.64* [116] 3.42 [117] 3.08 [118]	[80, 119–122]	Perovskite family *-computational band gap
AgNbO ₃	[123]	2.8 [124]	[80, 119, 125, 126]	Perovskite family
PbZrO ₃	[127]	3.7 [128–130]	[80, 119]	Perovskite family
PbHfO ₃	[131]	3.5* [132]	[80, 119, 133]	Perovskite type. Twins present, but investigation for ferroelastic behavior not carried out. *-computational band gap

its magnitude, it likely involves surface flexoelectric or surface ferroelectric states. Because polarization values of a few $\mu\text{C cm}^{-2}$ were shown computationally to result in significant performance improvements, these observations indicate a new direction to explore for photocatalyst design. Interestingly, both materials can be described as anti-ferroelectric ferroelastics, having a local dipolar unit in the unit cell ordered in an anti-parallel fashion. It is likely that these local dipolar groups are related to the spatially selective properties. Much work is needed to quantify the origin and magnitude of spatially selective polarization and reactivity in ferroelastics. However, because of the significant advantages that spatial separation of photogenerated charge carriers and electrochemical reaction sites have in the context of efficient photocatalysis, the possible identification of a new class of materials for photocatalyst design is of great interest for solar water splitting.

Acknowledgments

We acknowledge the support of the National Science Foundation grant DMR 1609369 and use of the Materials Characterization Facility at Carnegie Mellon University supported by grant MCF-677785.

ORCID iDs

Ajay S Pisat  <https://orcid.org/0000-0001-6671-8144>
 Gregory S Rohrer  <https://orcid.org/0000-0002-9671-3034>
 Paul A Salvador  <https://orcid.org/0000-0001-7106-0017>

References

- [1] Morrison S R 1980 *Electrochemistry at Semiconductor and Oxidized Metal Electrodes* (New York: Plenum) 978-1-4613-3146-9
- [2] Li J and Wu N 2015 Semiconductor-based photocatalysts and photoelectrochemical cells for solar fuel generation: a review *Catal. Sci. Technol.* **5** 1360–84
- [3] Zaleska A 2008 Doped-TiO₂: a review *Recent Patents Eng.* **2** 157–64
- [4] Li Z, Luo W, Zhang M, Feng J and Zou Z 2013 Photoelectrochemical cells for solar hydrogen production: current state of promising photoelectrodes, methods to improve their properties, and outlook *Energy Environ. Sci.* **6** 347–70
- [5] Haro M, Solis C, Molina G, Otero L, Bisquert J, Gimenez S and Guerrero A 2015 Toward stable solar hydrogen generation using organic photoelectrochemical cells *J. Phys. Chem. C* **119** 6488–94
- [6] Khaselev O and Turner J A 1998 A monolithic photovoltaic-photoelectrochemical device for hydrogen production via water splitting *Science* **280** 425–7
- [7] Jang J S, Kim H G and Lee J S 2012 Heterojunction semiconductors: a strategy to develop efficient photocatalytic materials for visible light water splitting *Catal. Today* **185** 270–7
- [8] Li H *et al* 2016 Forming heterojunction: an effective strategy to enhance the photocatalytic efficiency of a new metal-free organic photocatalyst for water splitting *Sci. Rep.* **6** 29327
- [9] Reza Gholipour M, Dinh C-T, Béland F and Do T-O 2015 Nanocomposite heterojunctions as sunlight-driven photocatalysts for hydrogen production from water splitting *Nanoscale* **7** 8187–208
- [10] Moniz S J A, Shevlin S A, Martin D J, Guo Z-X and Tang J 2015 Visible-light driven heterojunction photocatalysts for water splitting—a critical review *Energy Environ. Sci.* **8** 731–59

- [11] Marschall R 2014 Semiconductor composites: strategies for enhancing charge carrier separation to improve photocatalytic activity *Adv. Funct. Mater.* **24** 2421–40
- [12] Li L, Salvador P A and Rohrer G S 2014 Photocatalysts with internal electric fields *Nanoscale* **6** 24–42
- [13] Inoue Y, Sato K and Suzuki S 1985 Polarization effects upon adsorptive and catalytic properties: II. Surface electrical conductivity of nickel (II) oxide deposited on lithium niobate (LiNbO_3) and its changes *J. Phys. Chem.* **3** 2827–31
- [14] Inoue Y, Sato K and Miyama H 1986 Photoassisted water decomposition by ferroelectric lead zirconate titanate ceramics with anomalous photovoltaic effects *J. Phys.* **90** 2809–10
- [15] Inoue Y, Okamura M and Sato K 1985 A thin-film semiconducting titanium dioxide combined with ferroelectrics for photoassisted water decomposition *J. Phys. Chem.* **89** 5184–7
- [16] Giocondi J L and Rohrer G S 2000 Photochemical reduction and oxidation reactions on barium titanate surfaces *MRS Proc.* **654** 1–10
- [17] Giocondi J L and Rohrer G S 2001 Spatially selective photochemical reduction of silver on the surface of ferroelectric barium titanate *Chem. Mater.* **13** 241–2
- [18] Giocondi J L, Samadzadeh S and Rohrer G S 2003 Orientation dependence of the photochemical reactivity of BaTi_4O_9 *Mat. Res. Soc. Symp. Proc.* **755** 221–6
- [19] Bhardwaj A, Burbure N V and Rohrer G S 2010 Enhanced photochemical reactivity at the ferroelectric phase transition in $\text{Ba}_{1-x}\text{Sr}_x\text{TiO}_3$ *J. Am. Ceram. Soc.* **93** 4129–34
- [20] Bhardwaj A, Burbure N V, Gamalski A and Rohrer G S 2010 Composition dependence of the photochemical reduction of Ag by $\text{Ba}_{1-x}\text{Sr}_x\text{TiO}_3$ *Chem. Mater.* **22** 3527–34
- [21] Burbure N V, Salvador P A and Rohrer G S 2010 Photochemical reactivity of titania films on BaTiO_3 substrates: influence of titania phase and orientation *Chem. Mater.* **22** 5831–7
- [22] Tiwari D and Dunn S 2009 Photochemistry on a polarisable semi-conductor: what do we understand today? *J. Mater. Sci.* **44** 5063–79
- [23] Zhu Y, Salvador P A and Rohrer G S 2016 Controlling the relative areas of photocathodic and photoanodic terraces on the SrTiO_3 (111) Surface *Chem. Mater.* **28** 5155–62
- [24] Zhu Y, Salvador P A and Rohrer G S 2017 Buried charge at the $\text{TiO}_2/\text{SrTiO}_3$ (111) interface and its effect on photochemical reactivity *ACS Appl. Mater. Interfaces* **3** 7843–51
- [25] Li L, Liu X, Zhang Y, Nuhfer N T, Barmak K, Salvador P A and Rohrer G S 2013 Visible-light photochemical activity of heterostructured core-shell materials composed of selected ternary titanates and ferrites coated by TiO_2 *ACS Appl. Mater. Interfaces* **5** 5064–71
- [26] Li L, Zhang Y, Schultz A M, Liu X, Salvador P A and Rohrer G S 2012 Visible light photochemical activity of heterostructured PbTiO_3 - TiO_2 core-shell particles *Catal. Sci. Technol.* **2** 1945–52
- [27] Li L, Liu X, Zhang Y, Salvador P A and Rohrer G S 2013 Heterostructured $(\text{Ba,Sr})\text{TiO}_3/\text{TiO}_2$ core/shell photocatalysts: Influence of processing and structure on hydrogen production *Int. J. Hydrogen Energy* **38** 6948–59
- [28] Li L, Rohrer G S and Salvador P A 2012 Heterostructured ceramic powders for photocatalytic hydrogen production: Nanostructured TiO_2 shells surrounding microcrystalline $(\text{Ba, Sr})\text{TiO}_3$ cores *J. Am. Ceram. Soc.* **95** 1414–20
- [29] Zhang Y, Schultz A M, Salvador P A and Rohrer G S 2011 Spatially selective visible light photocatalytic activity of $\text{TiO}_2/\text{BiFeO}_3$ heterostructures *J. Mater. Chem.* **21** 4168–74
- [30] Burbure N V, Salvador P A and Rohrer G S 2010 Photochemical reactivity of titania films on BaTiO_3 substrates: origin of spatial selectivity *Chem. Mater.* **22** 5823–30
- [31] Liao L *et al* 2014 Efficient solar water-splitting using a nanocrystalline CoO photocatalyst *Nat. Nanotechnol.* **9** 69–73
- [32] Liu C, Tang J, Chen H M, Liu B and Yang P 2013 A fully integrated nanosystem of semiconductor nanowires for direct solar water splitting *Nano Lett.* **13** 2989–92
- [33] Lewis N S 2016 Developing a scalable artificial photosynthesis technology through nanomaterials by design *Nat. Nanotechnol.* **11** 1010–9
- [34] Osterloh F E 2008 Inorganic materials as catalysts for photoelectrochemical splitting of water *Chem. Mater.* **20** 35–54
- [35] Kudo A and Miseki Y 2009 Heterogeneous photocatalyst materials for water splitting *Chem. Soc. Rev.* **38** 253–78
- [36] Reece S Y, Hamel J A, Sung K, Jarvi T D, Esswein A J, Pijpers J J H and Nocera D G 2011 Wireless solar water splitting using silicon-based semiconductors and earth-abundant catalysts *Science* **334** 645–8
- [37] Kalisman P, Nakibli Y and Amirav L 2016 Perfect photon-to-hydrogen conversion efficiency *Nano Lett.* **16** 1776–81
- [38] Jiang X, Wang P and Zhao J 2015 2D covalent triazine framework: a new class of organic photocatalyst for water splitting *J. Mater. Chem. A* **3** 7750–8
- [39] Guerrero A, Haro M, Bellani S, Antognazza M R, Meda L, Gimenez S and Bisquert J 2014 Organic photoelectrochemical cells with quantitative photocarrier conversion *Energy Environ. Sci.* **7** 3666–73
- [40] Esiner S, Willems R E M, Furlan A, Li W, Wienk M M and Janssen R A J 2015 Photoelectrochemical water splitting in an organic artificial leaf *J. Mater. Chem. A* **3** 23936–45
- [41] Martin D J, James P, Reardon T, Moniz S J A and Tang J 2014 Visible light-driven pure water splitting by a nature-inspired organic semiconductor based system *J. Am. Chem. Soc.* **136** 12568–71
- [42] Liu C, Ziesack M, Silver P A and Nocera D G 2016 Water splitting—biosynthetic system with CO_2 reduction efficiencies exceeding photosynthesis *Science* **352** 1210–3
- [43] Nocera D G 2012 The artificial leaf *Acc. Chem. Res.* **45** 767–76
- [44] Sathre R, Scown C D, Morrow W R, Stevens J C, Sharp I D, Ager J W, Walczak K, Houle F A and Greenblatt J B 2014 Life-cycle net energy assessment of large-scale hydrogen production via photoelectrochemical water splitting *Energy Environ. Sci.* **7** 3264–78
- [45] Dunn S 2011 Time to think outside the box: new routes to water splitting *Mater. Today* **14** 302
- [46] Sapriel J 1975 Domain-wall orientations in ferroelastics *Phys. Rev. B* **12** 5128–40
- [47] Kalinin S V, Bonnell D A, Alvarez T, Lei X, Hu Z, Ferris J H, Zhang Q and Dunn S 2002 Atomic polarization and local reactivity on ferroelectric surfaces: a new route toward complex nanostructures *Nano Lett.* **2** 589–93
- [48] Wenderich K and Mul G 2016 Methods, mechanism, and applications of photodeposition in photocatalysis: a review *Chem. Rev.* **116** 14587–619
- [49] Giocondi J L and Rohrer G S 2001 Spatial separation of photochemical oxidation and reduction reactions on the surface of ferroelectric BaTiO_3 *J. Phys. Chem. B* **105** 8275–7
- [50] Giocondi J L and Rohrer G S 2008 The influence of the dipolar field effect on the photochemical reactivity of $\text{Sr}_2\text{Nb}_2\text{O}_7$ and BaTiO_3 microcrystals *Top. Catal.* **49** 18–23
- [51] Munprom R, Salvador P A and Rohrer G S 2016 Ferroelastic domains improve photochemical reactivity: a comparative study of monoclinic and tetragonal $(\text{Bi}_{1-0.5x}\text{Na}_{0.5x})(\text{V}_{1-x}\text{Mo}_x)\text{O}_4$ ceramics *J. Mater. Chem. A* **4** 2951–9

- [52] Munprom R, Salvador P A and Rohrer G S 2014 Polar domains at the surface of centrosymmetric BiVO_4 *Chem. Mater.* **26** 2774–6
- [53] Schultz A M, Zhang Y, Salvador P A and Rohrer G S 2011 Effect of crystal and domain orientation on the visible-light photochemical reduction of Ag on BiFeO_3 *ACS Appl. Mater. Interfaces* **3** 1562–7
- [54] Kalinin S V, Johnson C Y and Bonnell D A 2002 Domain polarity and temperature induced potential inversion on the BaTiO_3 (100) surface *J. Appl. Phys.* **91** 3816–23
- [55] Burbure N V, Salvador P A and Rohrer G S 2006 Influence of dipolar fields on the photochemical reactivity of thin titania films on BaTiO_3 substrates *J. Am. Ceram. Soc.* **89** 2943–5
- [56] Munprom R, Salvador P A and Rohrer G S 2015 The orientation dependence of the photochemical reactivity of BiVO_4 *J. Mater. Chem. A* **3** 2370–7
- [57] Giocondi J L, Salvador P A and Rohrer G S 2007 The origin of photochemical anisotropy in SrTiO_3 *Top. Catalysis* **44** 529–33
- [58] Mu L *et al* 2016 Enhancing charge separation on high symmetry SrTiO_3 exposed with anisotropic facets for photocatalytic water splitting *Energy Environ. Sci.* **9** 2463–9
- [59] Li G, Yi Z, Bai Y, Zhang W and Zhang H 2012 Anisotropy in photocatalytic oxidation activity of NaNbO_3 photocatalyst *Dalton Trans.* **41** 10194–8
- [60] Hu Y H, Chan H M, Wen Z X and Harmer M P 1975 Scanning electron microscopy and transmission electron microscopy study of ferroelectric domains in doped BaTiO_3 *J. Am. Ceram. Soc.* **69** 594–602
- [61] Stock M and Dunn S 2011 LiNbO_3 -a new material for artificial photosynthesis *IEEE Trans. Ultrason. Ferroelectr. Freq. Control* **58** 1988–93
- [62] Morris M R, Pendlebury S R, Hong J, Dunn S and Durrant J R 2016 Effect of internal electric fields on charge carrier dynamics in a ferroelectric material for solar energy conversion *Adv. Mater.* **28** 7123–8
- [63] Dunn S and Tiwari D 2008 Influence of ferroelectricity on the photoelectric effect of LiNbO_3 *Appl. Phys. Lett.* **93** 092905
- [64] Jones P M and Dunn S 2009 Interaction of Stern layer and domain structure on photochemistry of lead-zirconate-titanate *J. Phys. D: Appl. Phys.* **42** 065408
- [65] Cui Y, Briscoe J and Dunn S 2013 Effect of ferroelectricity on solar-light-driven photocatalytic activity of BaTiO_3 —influence on the carrier separation and stern layer formation *Chem. Mater.* **25** 4215–23
- [66] Kumar A *et al* 2008 Linear and nonlinear optical properties of BiFeO_3 *Appl. Phys. Lett.* **92** 121915
- [67] Bierlein J D and Sleight A W 1975 Ferroelasticity in BiVO_4 *Solid State Commun.* **16** 69–70
- [68] Toledano P and Guennou M 2016 Theory of antiferroelectric phase transitions *Phys. Rev. B* **94** 014107
- [69] Pisat A S, Rohrer G S and Salvador P A 2017 Spatial selectivity of Ag^+ reduction on polar surfaces of ferroelastic $\gamma\text{-WO}_3$ *J. Mater. Chem. A* **5** 8261–6
- [70] Aird A and Salje E K H 2000 Enhanced reactivity of domain walls in WO_3 with sodium *Eur. Phys. J. B* **15** 205–10
- [71] Ueda R and Ichinokawa T 1950 Domain structure of tungsten trioxide *Phys. Rev.* **80** 1106
- [72] Ueda R and Kobayashi J 1953 Antiparallel dipole arrangement in tungsten trioxide *Phys. Rev.* **91** 1565
- [73] Tanisaki S 1958 Effect of external stress on the domain structure of WO_3 *J. Phys. Soc. Japan* **13** 363–6
- [74] Yun S *et al* 2015 Ferroelastic twin structures in epitaxial WO_3 thin films *Appl. Phys. Lett.* **107** 252904
- [75] Kim Y, Alexe M and Salje E K H 2010 Nanoscale properties of thin twin walls and surface layers in piezoelectric WO_{3-x} *Appl. Phys. Lett.* **96** 032904
- [76] Yang W, Yu Y, Starr M B, Yin X, Li Z, Kvit A, Wang S, Zhao P and Wang X 2015 Ferroelectric polarization-enhanced photoelectrochemical water splitting in $\text{TiO}_2\text{-BaTiO}_3$ core-shell nanowire photoanodes *Nano Lett.* **15** 7574–80
- [77] Glickstein J J, Salvador P A and Rohrer G S 2016 Computational model of domain-specific reactivity on coated ferroelectric photocatalysts *J. Phys. Chem. C* **120** 12673–84
- [78] Glickstein J J, Salvador P A and Rohrer G S 2016 Multidomain simulations of coated ferroelectrics exhibiting spatially selective photocatalytic activity with high internal quantum efficiencies *J. Mater. Chem. A* **4** 16085–93
- [79] Zubko P, Catalan G and Tagantsev A K 2013 Flexoelectric effect in solids *Annu. Rev. Mater. Res.* **43** 387–421
- [80] Rabe K 2013 *Antiferroelectricity in Oxides: A Reexamination Functional Metal Oxides: New Science and Novel Applications* (Weinheim-VCH: Wiley) pp 221–44
- [81] Roy Chaudhuri A, Arredondo M, Hähnel A, Morelli A, Becker M, Alexe M and Vrejoiu I 2011 Epitaxial strain stabilization of a ferroelectric phase in PbZrO_3 thin films *Phys. Rev. B* **84** 054112
- [82] Boldyreva K, Pintilie L, Lotnyk A, Misirliglu I B, Alexe M and Hesse D 2007 Thickness-driven antiferroelectric-to-ferroelectric phase transition of thin PbZrO_3 layers in epitaxial $\text{PbZrO}_3/\text{Pb}(\text{Zr}_{0.8}\text{Ti}_{0.2})\text{O}_3$ multilayers *Appl. Phys. Lett.* **91** 122915
- [83] Reyes-Lillo S E and Rabe K M 2013 Antiferroelectricity and ferroelectricity in epitaxially strained PbZrO_3 from first principles *Phys. Rev. B* **88** 180102
- [84] Mani B K, Chang C M, Lisenkov S and Ponomareva I 2015 Critical thickness for antiferroelectricity in PbZrO_3 *Phys. Rev. Lett.* **115** 097601
- [85] Uchino K 2016 Antiferroelectric shape memory ceramics *Actuators* **5** 11
- [86] Ayyub P, Chattopadhyay S, Pinto R and Multani M S 1998 Ferroelectric behavior in thin films of antiferroelectric materials *Phys. Rev. B* **57** R5559–62
- [87] Mirshekarloo M S, Yao K and Sritharan T 2012 Ferroelastic strain induced antiferroelectric-ferroelectric phase transformation in multilayer thin film structures *Adv. Funct. Mater.* **22** 4159–64
- [88] Tagantsev A K *et al* 2013 The origin of antiferroelectricity in PbZrO_3 *Nat. Commun.* **4** 2229
- [89] Hamdi H, Ghosez P and Bousquet E 2016 First-principles Re-investigation of bulk WO_3 *Phys. Rev. B* **94** 245124
- [90] Woodward P M, Sleight A W and Vogt T 1997 Ferroelectric tungsten trioxide *J. Solid State Chem.* **131** 9–17
- [91] Cooper J K, Gul S, Toma F M, Chen L, Liu Y S, Guo J, Ager J W, Yano J and Sharp I D 2015 Indirect bandgap and optical properties of monoclinic bismuth vanadate *J. Phys. Chem. C* **119** 2969–74
- [92] Dunkle S S, Helmich R J and Suslick K S 2009 BiVO_4 as a visible-light photocatalyst prepared by ultrasonic spray pyrolysis *J. Phys. Chem. C* **113** 11980–3
- [93] Bamwenda G R and Arakawa H 2016 The visible light induced photocatalytic activity of tungsten trioxide powders *Appl. Catalysis A* **210** 181–91
- [94] Baek B S *et al* 2011 Nature of polarization fatigue in BiFeO_3 *Adv. Mater.* **23** 1621–5
- [95] Graf M, Sepiarsky M, Tinte S and Stachiotti M G 2014 Phase transitions and antiferroelectricity in BiFeO_3 from atomic-level simulations *Phys. Rev. B* **90** 184108
- [96] Kan D, Pálová L, Anbusathaiah V, Cheng C J, Fujino S, Nagarajan V, Rabe K M and Takeuchi I 2010 Universal behavior and electric-field-induced structural transition in rare-earth-substituted BiFeO_3 *Adv. Funct. Mater.* **20** 1108–15
- [97] Muñoz-Saldaña J, Schneider G A and Eng L M 2001 Stress induced movement of ferroelastic domain walls in BaTiO_3 single crystals evaluated by scanning force microscopy *Surf. Sci.* **480** L402–10

- [98] Yun S 2011 Double hysteresis loop in BaTiO₃-based ferroelectric ceramics *Ferroelectrics—Characterization and Modeling* (Rijeka: INTECH) pp 245–64
- [99] Zhang Q, Cagin T and Goddard W A 2006 The ferroelectric and cubic phases in BaTiO₃ ferroelectrics are also antiferroelectric *Proc. Natl Acad. Sci. USA* **103** 14695–700
- [100] Lawless W N 1967 Ferroelectricity and antiferroelectricity in BaTiO₃ *J. Phys. Soc. Japan* **23** 325–31
- [101] Sleight A and Jones G 1975 Ferroelastic transitions in β -BiNbO₄ and β -BiTaO₄ *Acta Cryst.* **B31** 2748–9
- [102] Zou Z, Ye J, Sayama K and Arakawa H 2001 Photocatalytic and photophysical properties of a novel series of solid photocatalysts, BiTa_{1-x}Nb_xO₄ (0 ≤ x ≤ 1) *Chem. Phys. Lett.* **343** 303–8
- [103] Popolitov V I, Lobachev A N and Peskin V F 1982 Antiferroelectrics, ferroelectrics and pyroelectrics of a stibiotantalite structure *Ferroelectrics* **40** 9–16
- [104] Nisar J, Almeida Silva L, Gomes Almeida C, Santos Mascarenhas J A, Wang B, Moysés Araújo C, Ahuja R, Pepe I, Souza de Almeida J and Ferreira da Silva A 2012 Study of electronic and optical properties of BiTaO₄ for photocatalysis *Phys. Status Solidi Curr. Top. Solid State Phys.* **9** 1593–6
- [105] Popolitov V I, Ivanova L A, Stephanovitch S Y, Chetchkin V V, Lobachev A N and Venetsev Y N 1974 Ferroelectrics abo4: synthesis of single crystals and ceramics; dielectric and nonlinear optical properties *Ferroelectrics* **8** 519–20
- [106] Vullum F, Nitsche F, Selbach S M and Grande T 2008 Solid solubility and phase transitions in the system LaNb_{1-x}Ta_xO₄ *J. Solid State Chem.* **181** 2580–5
- [107] Machida M, Murakami S, Kijima T, Matsushima S and Arai M 2001 Photocatalytic property and electronic structure of lanthanide tantalates, LnTaO₄ (Ln = La, Ce, Pr, Nd, and Sm) *J. Phys. Chem. B* **105** 3289–94
- [108] Abreu Y G, Siqueira K P F, Matinaga F M, Moreira R L and Dias A 2017 High-temperature antiferroelectric and ferroelectric phase transitions in phase pure LaTaO₄ *Ceram. Int.* **43** 1543–51
- [109] Safari A and Akdogan E K 2007 *Piezoelectric Transducers and Acoustic Materials for Transducer Applications* (USA: Springer) 978-0-387-76540-2
- [110] Zhou S, Weng Y, Wu Z, Wang J, Wu L, Ni Z, Xu Q and Dong S 2016 Strong room-temperature blue-violet photoluminescence of multiferroic BaMnF₄ *Phys. Chem. Chem. Phys.* **18** 2054–8
- [111] Scott J F 1979 Phase transitions in BaMnF₄ *Rep. Prog. Phys.* **12** 1055–84
- [112] Hidaka M, Nakayama T, Scott J F and Storey J S 1987 Antiferroelectric short-range order of BaMnF₄ *Physica B* **144** 310–9
- [113] Molak A and Kubacki J 2001 Structure of NaNbO₃:xMn single crystals at room temperature *Cryst. Res. Technol.* **36** 893–902
- [114] Molak A, Pawelczyk M and Onodera A 1995 Specific heat and axial pressure influence on phase transitions in NaNbO₃:Mn *Ferroelectrics* **172** 295–8
- [115] Molak A, Pawelczyk M and Kwapulinski J 1994 Changes in structure and electrical properties of NaNbO₃ induced by Mn dopant *J. Phys.: Condens. Matter* **6** 6833–42
- [116] Modak B, Modak P and Ghosh S K 2016 Improving visible light photocatalytic activity of NaNbO₃: a DFT based investigation *RSC Adv.* **6** 90188–96
- [117] Li P, Abe H and Ye J 2014 Band-gap engineering of NaNbO₃ for photocatalytic H₂ evolution with visible light *Int. J. Photoenergy* **2014** 380421
- [118] Liu J W, Chen G, Li Z H and Zhang Z G 2007 Hydrothermal synthesis and photocatalytic properties of ATaO₃ and ANbO₃ (A = Na and K) *Int. J. Hydrogen Energy* **32** 2269–72
- [119] Subbarao E C 1973 Ferroelectric and antiferroelectric materials *Ferroelectrics* **5** 267–80
- [120] Mishra S K, Choudhury N, Chaplot S L, Krishna P S R and Mittal R 2007 Competing antiferroelectric and ferroelectric interactions in NaNbO₃: neutron diffraction and theoretical studies *Phys. Rev. B* **76** 024110
- [121] Xu Y, Hong W, Feng Y and Tan X 2014 Antiferroelectricity induced by electric field in NaNbO₃-based lead-free ceramics *Appl. Phys. Lett.* **104** 052903
- [122] Ji S, Liu H, Sang Y, Liu W, Yu G and Leng Y 2014 Synthesis, structure, and piezoelectric properties of ferroelectric and antiferroelectric NaNbO₃ nanostructures *CrystEngComm* **16** 7598–604
- [123] Miga S and Dec J 1999 Reorientation of the W' domain walls in ferroelastic silver niobate crystal *J. Appl. Phys.* **85** 1756–9
- [124] Yang L, Liu J, Chang H and Tang S 2015 Enhancing the visible-light-induced photocatalytic activity of AgNbO₃ by loading Ag@AgCl nanoparticles *RSC Adv.* **5** 59970–5
- [125] Sakurai H, Yamazoe S and Wada T 2010 Ferroelectric and antiferroelectric properties of AgNbO₃ films fabricated on (001), (110), and (111) SrTiO₃ substrates by pulsed laser deposition *Appl. Phys. Lett.* **97** 042901
- [126] Zhao L, Liu Q, Zhang S and Li J-F 2016 Lead-free AgNbO₃ anti-ferroelectric ceramics with an enhanced energy storage performance using MnO₂ modification *J. Mater. Chem. C* **4** 8380–4
- [127] H Ekhard K S and Salje E K H 2000 Mesoscopic twin patterns in ferroelastic and co-elastic minerals *Rev. Mineral. Geochem.* **39** 65–84
- [128] Robertson J 2000 Band offsets of wide-band-gap oxides and implications for future electronic devices *J. Vac. Sci. Technol. B* **18** 1785
- [129] Moret M P, Devillers M A C, Wörhoff K and Larsen P K 2002 Optical properties of PbTiO₃, PbZr_xTi_{1-x}O₃, PbZrO₃ films deposited by metalorganic chemical vapor on SrTiO₃ *J. Appl. Phys.* **92** 468–74
- [130] Peng C H, Chang J-F and Desu S B 1991 Optical Properties of PZT, PLZT, and PNZT Thin Films *MRS Proc.* **243** 21–6
- [131] Topolov V Y, Balyunis L E, Turik A V and Fesenko O E 1990 The specifics of twinning in orthorhombic phases of PbHfO₃ single crystals *Ferroelectrics* **110** 41–5
- [132] Hautier G, Miglio A, Ceder G, Rignanese G-M and Gonze X 2013 Identification and design principles of low hole effective mass p-type transparent conducting oxides *Nat. Commun.* **4** 2292
- [133] Shirane G and Pepinsky R 1953 Phase transitions in antiferroelectric PbHfO₃ *Phys. Rev.* **91** 812–5
- [134] Gonzalo J A and Jiménez B 2008 *Ferroelectricity The Fundamentals Collection* (Weinheim: Wiley-VCH) 978-3-527-61801-9
- [135] Wang F, Grinberg I and Rappe A M 2014 Band gap engineering strategy via polarization rotation in perovskite ferroelectrics *Appl. Phys. Lett.* **104** 152903
- [136] He J, Franchini C and Rondinelli J M 2016 Ferroelectric oxides with strong visible-light absorption from charge ordering *Chem. Mater.* **29** 2445–51
- [137] Zhao Z, Ding X, Sun J and Salje E K H 2014 Thermal and athermal crackling noise in ferroelastic nanostructures *J. Phys.: Condens. Matter* **26** 142201
- [138] Ullah R, Ang H M, Tadó M O and Wang S 2012 Synthesis of doped BiNbO₄ photocatalysts for removal of gaseous volatile organic compounds with artificial sunlight *Chem. Eng. J.* **185–186** 328–36
- [139] Zhai H-F, Li A-D, Kong J-Z, Li X-F, Zhao J, Guo B-L, Yin J, Li Z-S and Wu D 2013 Preparation and visible-light photocatalytic properties of BiNbO₄ and BiTaO₄ by a citrate method *J. Solid State Chem.* **202** 6–14
- [140] Ullah R, Sun H, Ang H M, Tadó M O and Wang S 2012 Photocatalytic oxidation of water and air contaminants with

- metal doped BiTaO₄ irradiated with visible light *Catal. Today* **192** 203–12
- [141] Li G, Yan S, Wang Z, Wang X, Li Z, Ye J and Zou Z 2009 Synthesis and visible light photocatalytic property of polyhedron-shaped AgNbO₃ *Dalton Trans.* **3** 8519–24
- [142] Wadhawan V K 1984 Ferroelasticity *Bull. Mater. Sci.* **6** 733–53
- [143] Bursian E V 2004 The importance of the unlocal piezoeffect in domain structure formation in ferroelectrics *Ferroelectrics* **307** 177–9